

# NLO QCD corrections to same-sign $T$ -odd quark pair production in the littlest Higgs model with $T$ -parity at the LHC

Xiong Shou-Jian, Ma Wen-Gan, Guo Lei, Chen Chong, and Zhang Ren-You

Department of Modern Physics, University of Science and Technology

of China (USTC), Hefei, Anhui 230026, P.R.China

## Abstract

We present the calculations for the same-sign  $T$ -odd mirror quark pair production of the first two generations in the littlest Higgs model with  $T$ -parity (LHT) at the  $\sqrt{s} = 14$  TeV LHC up to the QCD next-to-leading order (NLO) including the subsequent decays of the  $T$ -odd mirror quarks. The uncertainties from the factorization/renormalization scale and parton distribution functions (PDFs) are discussed. Our numerical results show that the PDF uncertainty of the NLO QCD corrected cross section for the same-sign  $T$ -odd mirror quark pair production of the first two generations is comparable with the scale uncertainty, and the combined uncertainty at the QCD NLO is much smaller than that at the LO with the factorization/renormalization scale  $\mu$  in the range of  $[\mu_0/4, 4\mu_0]$ . We also study the dependence of the total cross section on the LHT parameters, and provide the transverse momentum, rapidity, invariant mass and  $H_T$  distributions of final products.

**PACS:** 12.38.Bx, 13.85.Dz, 13.66.Hk

## I. Introduction

Although the standard model (SM) [1, 2] has been repeatedly confirmed by high energy experiments, there are still a number of theoretical problems unsolved, providing strong motivations to search for physics beyond the SM. As one of them, the fine-tuning problem of the Higgs boson [3] has become even more attractive after the discovery of the 126 GeV Higgs boson by the ATLAS and CMS collaborations [4, 5]. To regulate quadratically divergent contributions to the Higgs mass, many extended models are proposed. Among them, the little Higgs models [6] deserve attention due to their constructions as one kind of electroweak symmetry breaking (EWSB) without fine-tuning problem. The Higgs boson in these models manifests as a Nambu-Goldstone boson corresponding to a new global symmetry, which guarantees the lightness of the Higgs boson through its spontaneous breaking at a higher scale  $f$ .

The most economical version of the little Higgs models is the littlest Higgs model (LHM) [7]. In addition to the SM particle spectrum, a set of new heavy gauge bosons ( $W_H^\pm, Z_H, A_H$ ), a colored vector-like quark ( $T$ ) and a scalar triplet ( $\Phi$ ) are introduced in the LHM. Unfortunately, the original construction of the LHM conflicts severely with precision electroweak constraints [8], forcing the value of  $f$  to be as large as several TeV. The fine-tuning between the cutoff scale  $4\pi f$  and the weak scale will be needed again for a too large  $f$  value. This problem can be solved naturally when the LHM is endowed a discrete symmetry named  $T$ -parity [9, 10, 11]. In the littlest Higgs model with  $T$ -parity (LHT), newly introduced particles are odd under  $T$ -parity except  $T_+$ , while the SM particles are  $T$ -even.  $T$ -parity conservation makes the  $T$ -odd particles can only be produced in pairs, and the SM gauge bosons can not mix with their  $T$ -partners. Hence the new particles do not contribute to the electroweak precision observables at tree level, then all such corrections from new particles are loop suppressed and small. All of these allow a relatively low value of  $f$ . According to the latest results from the 8 TeV run at the LHC, the constraints from Higgs couplings are by now competing with electroweak precision tests and both combined exclude  $f$  up to 694 GeV or 560 GeV depending on the implementation of the down-type Yukawa sector [13]. With the new particles and a relatively low value of  $f$ , rich phenomena of the LHT can be expected at the LHC. Another interesting thing predicted in the LHT is that the neutral and colorless weakly interacting stable  $T$ -odd  $A_H$  can be a good candidate for dark matter, which is also one of the problems unsolved in current particle physics.

The phenomenological study in the LHT is extensive. A study on phenomenology of the LHT including effects of  $T$ -odd fermions at tree level was reported in Ref.[14]. The signals of  $T$ -odd quarks in the LHT were analysed in Ref.[15]. The  $W_H$  pair production and  $W_H Z_H$  production at the LHC were calculated up to the QCD NLO in Ref.[16] and Ref.[17], respectively. Calculations on a  $T$ -odd gauge boson production associated with a  $T$ -odd heavy quark at the LHC at the QCD NLO were presented in Ref.[18]. The production of same-sign dileptons via SM mechanism at the LHC is rather rare, therefore, it is a very helpful to choose the same-sign dilepton production to search for the evidence of the LHT. Both the ATLAS and CMS collaborations have adopted same-sign dilepton events to search for new physics at the  $\sqrt{s} = 7$  TeV LHC (LHC7) and the  $\sqrt{s} = 8$  TeV LHC (LHC8) [19, 20]. By analyzing these signatures and other events from the ATLAS at the LHC8, J. Reuter, *et al.* provided robust and complementary LHT limits and constrained  $f$  to be larger than 638 GeV [13]. In this work we study the same-sign  $T$ -odd mirror quark pair production of the first two generations followed by the subsequent decay  $q_- \rightarrow W_H q' \rightarrow W A_H q' \rightarrow \ell \nu A_H q'$  up to the QCD NLO in the LHT at the  $\sqrt{s} = 14$  TeV LHC (LHC14). The rest of this paper is organized as follows: In Sec.II, we briefly review the related LHT theory. The calculation strategy is presented in Sec.III. The numerical results and discussions are provided in Sec.IV, and finally a short summary is given in Sec.V.

## II. Related LHT theory

In this section, we introduce briefly the LHT theory related to our study. For the detailed LHT theory one can refer to the literatures [9, 10, 11, 12]. The LHT is a nonlinear  $\sigma$  model based on a  $SU(5)$  global symmetry, in which a subgroup  $[SU(2)_1 \times U(1)_1] \times [SU(2)_2 \times U(1)_2]$  is gauged. At an energy scale of  $f \sim 1$  TeV, the  $SU(5)$  global symmetry spontaneously breaks down to its  $SO(5)$  subgroup. This symmetry breaking originates from the vacuum expectation value (VEV) of an  $SU(5)$  symmetric tensor field  $\Sigma$ , written as

$$\Sigma_0 = \langle \Sigma \rangle = \begin{pmatrix} & & 1_{2 \times 2} \\ & 1 & \\ 1_{2 \times 2} & & \end{pmatrix}. \quad (2.1)$$

This breaking gives rise to 14 Nambu-Goldstone (NG) bosons. Simultaneously, the gauged symmetry  $[SU(2)_1 \times U(1)_1] \times [SU(2)_2 \times U(1)_2]$  breaks down to the SM  $SU(2)_L \times U(1)_Y$  symmetry. A “pion”

matrix  $\Pi$  is employed to describe the 14 NG bosons as

$$\Pi = \begin{pmatrix} -\frac{\omega^0}{2} - \frac{\eta}{\sqrt{20}} & -\frac{\omega^+}{\sqrt{2}} & -i\frac{\pi^+}{\sqrt{2}} & -i\phi^{++} & -i\frac{\phi^+}{\sqrt{2}} \\ -\frac{\omega^-}{\sqrt{2}} & \frac{\omega^0}{2} - \frac{\eta}{\sqrt{20}} & \frac{v+h+i\pi^0}{2} & -i\frac{\phi^+}{\sqrt{2}} & \frac{-i\phi^0+\phi^P}{\sqrt{2}} \\ i\frac{\pi^-}{\sqrt{2}} & \frac{v+h-i\pi^0}{2} & \sqrt{4/5}\eta & -i\frac{\pi^+}{\sqrt{2}} & \frac{v+h+i\pi^0}{2} \\ i\phi^{--} & i\frac{\phi^-}{\sqrt{2}} & i\frac{\pi^-}{\sqrt{2}} & -\frac{\omega^0}{2} - \frac{\eta}{\sqrt{20}} & -\frac{\omega^-}{\sqrt{2}} \\ i\frac{\phi^-}{\sqrt{2}} & \frac{i\phi^0+\phi^P}{\sqrt{2}} & \frac{v+h-i\pi^0}{2} & -\frac{\omega^+}{\sqrt{2}} & \frac{\omega^0}{2} - \frac{\eta}{\sqrt{20}} \end{pmatrix}, \quad (2.2)$$

where  $(-i\pi^+/\sqrt{2}, (v+h+i\pi^0)/2)^T$  is the  $T$ -even  $SU(2)$  Higgs doublet, identified as the SM Higgs doublet, i.e.,  $h$  is the usual SM Higgs field,  $v = 246$  GeV is the Higgs VEV, and  $\pi^+, \pi^0$  are Goldstone bosons eaten by the SM  $W, Z$  bosons, respectively. The fields  $\eta$  and  $\omega$  are additional Goldstone bosons, and  $\Phi$  is a  $T$ -odd physical scalar triplet with components of  $\phi^{++}, \phi^+, \phi^0$  and  $\phi^P$ .

From the symmetry breaking by the VEV  $\Sigma_0$ , the  $T$ -odd gauge bosons  $A_H, Z_H$  and  $W_H$  get masses as

$$m_{A_H} \simeq \frac{1}{\sqrt{5}}g'f \left(1 - \frac{5}{8}\frac{v^2}{f^2}\right), \quad m_{W_H} \simeq m_{Z_H} \simeq gf \left(1 - \frac{1}{8}\frac{v^2}{f^2}\right). \quad (2.3)$$

The mass of the additional physical scalar triplet is given by

$$m_\Phi = \sqrt{2}m_h \frac{f}{v}, \quad (2.4)$$

where  $m_h$  is the mass of the SM Higgs boson, and all components of the triplet  $\Phi$  are degenerate at the order of  $\mathcal{O}\left(\frac{v^2}{f^2}\right)$ . In principle, the triplet  $\Phi$  can contribute to our investigated subprocesses, but the  $\bar{q}_-\Phi q$  coupling strengths are of  $\mathcal{O}(\frac{v^2}{f^2})$  [21]. Then the contributions to the amplitude involving such  $\bar{q}_-\Phi q$  interactions are suppressed by a factor of  $\frac{v^4}{f^4}$ . Therefore, we can ignore the effects induced by  $\bar{q}_-\Phi q$  interactions in this paper.

A consistent implementation of  $T$ -parity in the quark sector requires the introduction of the  $T$ -odd mirror quarks for the SM quarks. We denote the  $T$ -odd up- and down-type quarks as  $u_-^i$  and  $d_-^i$  ( $i = 1, 2, 3$ ), respectively. Assuming a universal and flavor independent Yukawa coupling  $\kappa$ , the masses of the  $T$ -odd heavy quarks are given by

$$m_{u_-^i} \simeq \sqrt{2}\kappa f \left(1 - \frac{1}{8}\frac{v^2}{f^2}\right), \quad m_{d_-^i} = \sqrt{2}\kappa f, \quad (i = 1, 2, 3). \quad (2.5)$$

The Feynman rules used in our calculations are listed in Table 1 [21]. We note that the  $T$ -odd mirror quark sector involves two Cabibbo-Kobayashi-Maskawa (CKM)-like unitary mixing matrices

$V_{Hu}$  and  $V_{Hd}$ , which satisfy  $V_{Hu}^\dagger V_{Hd} = V_{CKM}$  [21]. In the following calculations we take  $V_{CKM}$  to be a unit matrix, then we can take  $V_{Hu} = V_{Hd} = I$ .

Vertex	Feynman rule	Vertex	Feynman rule
$A_H^\mu \bar{u}_-^i u^j$	$-i \left( \frac{g'}{10} + \frac{g}{2} \sin \theta_H \right) (V_{Hu})_{ij} \gamma^\mu P_L$	$A_H^\mu \bar{d}_-^i d^j$	$i \left( -\frac{g'}{10} + \frac{g}{2} \sin \theta_H \right) (V_{Hd})_{ij} \gamma^\mu P_L$
$Z_H^\mu \bar{u}_-^i u^j$	$i \left( \frac{g}{2} - \frac{g'}{10} \sin \theta_H \right) (V_{Hu})_{ij} \gamma^\mu P_L$	$Z_H^\mu \bar{d}_-^i d^j$	$-i \left( \frac{g}{2} + \frac{g'}{10} \sin \theta_H \right) (V_{Hd})_{ij} \gamma^\mu P_L$
$\omega^0 \bar{u}_-^i u^j$	$\frac{g}{2m_{Z_H}} \left[ m_{u_-}^i \left( 1 + \frac{v^2}{8f^2} - \frac{\sin \theta_H}{\tan \theta_W} \right) P_L - m_{u_-}^j P_R \right] (V_{Hu})_{ij}$	$\omega^0 \bar{d}_-^i d^j$	$-\frac{g}{2m_{Z_H}} \left[ m_{d_-}^i \left( 1 - \frac{v^2}{4f^2} + \frac{\sin \theta_H}{\tan \theta_W} \right) P_L - m_{d_-}^j P_R \right] (V_{Hd})_{ij}$
$\eta \bar{u}_-^i u^j$	$-\frac{g'}{10m_{A_H}} \left[ m_{u_-}^i \left( 1 + \frac{5v^2}{8f^2} + \sin \theta_H \tan \theta_W \right) P_L - m_{u_-}^j P_R \right] (V_{Hu})_{ij}$	$\eta \bar{d}_-^i d^j$	$-\frac{g'}{10m_{A_H}} \left[ m_{d_-}^i \left( 1 - \frac{5v^2}{4f^2} + \sin \theta_H \tan \theta_W \right) P_L - m_{d_-}^j P_R \right] (V_{Hd})_{ij}$
$\bar{q}_-^\alpha q_-^\beta G_\mu^a$	$ig_s (T^a)_{\alpha\beta} \gamma^\mu$	$W^{+\mu} \bar{u}_-^i d_-^j$	$\frac{ig}{\sqrt{2}} \delta_{ij} \gamma^\mu$

Table 1: The related LHT Feynman rules used in this work, where  $q_- = u_-, d_-, c_-, s_-$ ,  $P_{L,R} = \frac{1}{2} (1 \mp \gamma_5)$ ,  $i$  and  $j$  are the generation indices.

### III. Calculation strategy

We calculate the same-sign  $T$ -odd mirror quark pair production of the first two generations at the LHC14 in the framework of the LHT up to the QCD NLO, including the  $T$ -odd quark subsequent decays. We use the developed FeynArts3.4 package [22] to generate Feynman diagrams and amplitudes under the t'Hooft Feynman gauge in the LHT, and employ FormCalc5.4 program [23] for algebraic manipulation. We use the Passarino-Veltman (PV) method to reduce a tensor integral to a linear combination of tensor structures and scalar coefficients. We adopt the expressions in Ref.[24] to deal with the IR singularities in loop integrals, and apply the expressions in Refs.[25, 26, 27] to implement the numerical evaluations for the IR-safe  $N$ -point integrals.

### III.1 LO cross section

The parton level processes, which contribute to the parent process  $pp \rightarrow q_- q'_- + X$  with  $q_-$  and  $q'_-$  same-sign charged, are denoted as

$$q(p_1) + q'(p_2) \rightarrow q_-(p_3) + q'_-(p_4), \quad (3.1)$$

where  $qq' = uu, \bar{d}\bar{d}, cc, \bar{s}\bar{s}, uc, \bar{d}\bar{s}, u\bar{d}, c\bar{s}, u\bar{s}, c\bar{d}$ , and their corresponding charge conjugations.  $p_i$  ( $i = 1, 2, 3, 4$ ) stand for the four-momenta of the incoming and outgoing particles. The LO partonic processes are all induced by EW interactions, and can be divided into four types: (i) The processes containing only  $t$ -channel Feynman diagrams. This type of partonic processes include  $uc \rightarrow u_- c_-$ ,  $\bar{d}\bar{s} \rightarrow \bar{d}_- \bar{s}_-$ ,  $u\bar{s} \rightarrow u_- \bar{s}_-$ ,  $c\bar{d} \rightarrow c_- \bar{d}_-$  and their corresponding charge conjugations. (ii) The processes involving  $s$ - and  $t$ -channel diagrams but no  $u$ -channel diagram. (iii) The processes containing  $u$ - and  $t$ -channel diagrams but no  $s$ -channel diagram. Each process of this type has identical two initial/final particles, such as  $uu \rightarrow u_- u_-$  partonic process. (iv) The processes containing only a  $s$ -channel Feynman diagram via  $W$ -exchange, i.e.,  $u\bar{d} \rightarrow c_- \bar{s}_-$ ,  $c\bar{s} \rightarrow u_- \bar{d}_-$  and their charge conjugations. We plot representative Feynman diagrams for the four types of partonic processes in Fig.1.

The LO cross section for the partonic process  $qq' \rightarrow q_- q'_-$  can be expressed as

$$\hat{\sigma}_{LO}(\hat{s}, qq' \rightarrow q_- q'_-) = \frac{1}{1 + \delta_{q_- q'_-}} \frac{1}{4} \frac{1}{9} \frac{(2\pi)^4}{2\hat{s}} \sum_{spin} \sum_{color} \int |\mathcal{M}_{LO}|^2 d\Omega_2, \quad (3.2)$$

where  $\frac{1}{4}$  and  $\frac{1}{9}$  are from averaging over the spins and colors of initial partons, and  $\frac{1}{1 + \delta_{q_- q'_-}}$  is due to the number of the identical  $T$ -odd quarks in final state.  $\sqrt{\hat{s}}$  is the partonic center-of-mass (c.m.) colliding energy and  $\mathcal{M}_{LO}$  is the LO amplitude for the partonic process  $qq' \rightarrow q_- q'_-$ . The two summations are taken over the spins and colors of all the relevant initial and final particles, separately. The integration is performed over the two-body phase space of the final particles  $q_-$  and  $q'_-$ , and  $d\Phi_2$  is the two-body phase space element defined as

$$d\Phi_2 = \delta^{(4)}(p_1 + p_2 - p_3 - p_4) \prod_{i=3}^4 \frac{d^3 \vec{p}_i}{(2\pi)^3 2E_i}. \quad (3.3)$$

The LO total cross section for the same-sign  $T$ -odd mirror quark pair production of all the first two generations at the LHC, denoted as  $\sigma_{LO}(pp \rightarrow q_- q'_- + X)$ , can be obtained as

$$\sigma_{LO}(pp \rightarrow q_- q'_- + X)$$

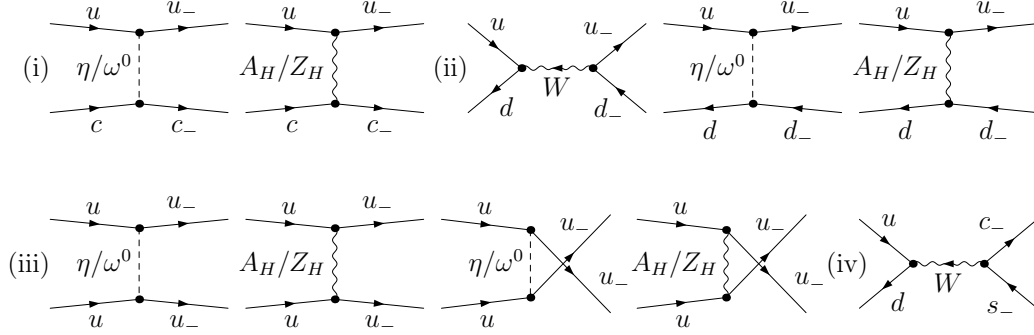


Figure 1: The representative LO Feynman diagrams for the partonic processes of type (i), (ii), (iii) and (iv), respectively.

$$= \sum_{qq'} \left\{ \int dx_A dx_B \left[ G_{q/A}(x_A, \mu_f) G_{q'/B}(x_B, \mu_f) \hat{\sigma}_{LO}(x_A x_B s, qq' \rightarrow q_- q'_-, \mu_f) + (A \leftrightarrow B) \right] \right\}, \quad (3.4)$$

where the summation is taken over all the partonic processes of the same-sign  $T$ -odd mirror quark pair production of the first two generations, i.e.,  $qq' = uu, \bar{u}\bar{u}, \bar{d}\bar{d}, dd, cc, \bar{c}\bar{c}, \bar{s}\bar{s}, ss, uc, \bar{u}\bar{c}, \bar{d}\bar{s}, ds, u\bar{d}, \bar{u}d, c\bar{s}, \bar{c}s, u\bar{s}, \bar{u}s, c\bar{d}, \bar{c}d$ .  $G_{i/P}$  ( $i = q, q', P = A, B$ ) is the parton distribution function (PDF) of parton  $i$  in proton  $P$ ,  $x_P$  is the momentum fraction of a parton in the proton  $P$ , and  $\mu_f$  is the factorization scale.

### III.2 NLO QCD corrections to $pp \rightarrow q_- q'_- + X$ process

The NLO QCD corrections to the  $pp \rightarrow q_- q'_- + X$  process involve the following components: (1) one-loop virtual corrections, (2) real gluon/light-quark emission corrections, and (3) PDF counterterm contributions. To regularize the ultraviolet (UV) and infrared (IR) divergences, the dimensional regularization scheme in  $D = 4 - 2\epsilon$  dimensions is employed. According to the Kinoshita-Lee-Nauenberg (KLN) [29] theorem, the sum of the above three components gives a IR-finite result.

The QCD one-loop level amplitudes for the partonic processes  $qq' \rightarrow q_- q'_-$  ( $qq' = uu, \bar{u}\bar{u}, \bar{d}\bar{d}, dd, cc, \bar{c}\bar{c}, \bar{s}\bar{s}, ss, uc, \bar{u}\bar{c}, \bar{d}\bar{s}, ds, u\bar{d}, \bar{u}d, c\bar{s}, \bar{c}s, u\bar{s}, \bar{u}s, c\bar{d}, \bar{c}d$ ) in the LHT are contributed by vertex and box Feynman diagrams. Both UV and IR singularities arise in the amplitudes. The UV divergence can be removed after performing the renormalization procedure. Since these partonic processes are EW induced, only the wave functions and masses of related colored particles need to be renormalized here. We adopt the renormalization constants defined in Ref.[18] and use the on-shell renormalization scheme. For the radiative processes, the phase space with soft and collinear singularities are separated

by adopting the two cutoff phase space slicing (TCPSS) method [28], which is intuitive, simple to implement, and relies on a minimum of process dependent information in the NLO calculations. The real gluon emission processes contain soft and collinear singularities, while the real light-quark emission processes contain only collinear singularities. The soft singularities in one-loop virtual corrections can be canceled by those in the real gluon emission processes exactly. The collinear singularities in the real gluon and light-quark emissions are canceled by those in the virtual corrections and corresponding PDF counterterms. The details about the PDF counterterms can be found in Ref.[28].

### III.3 NLO QCD corrected decay widths of $T$ -odd mirror quarks

We evaluate the impact of the terms of order  $(\alpha_s/\pi)m_{V_H}^2/m_{q_-}^2$  ( $V_H = Z_H, W_H, A_H$ ) on the decays of  $T$ -odd mirror quarks, and find that their contributions to the partial decay widths and branch ratios are below 0.2% and 0.01%, respectively. By neglecting the light quark masses and the terms of order  $(\alpha_s/\pi)m_{V_H}^2/m_{q_-}^2$ , the NLO QCD corrected partial decay width for the  $q_- \rightarrow V_H q'$  decay mode has the form as

$$\Gamma_{NLO}(q_- \rightarrow V_H q') = \Gamma_{LO}(q_- \rightarrow V_H q') \left[ 1 - \frac{2\alpha_s}{3\pi} \left( \frac{2\pi^2}{3} - \frac{5}{2} \right) \right],$$

$$(q_- = u_-, d_-, c_-, s_-, \bar{u}_-, \bar{d}_-, \bar{c}_-, \bar{s}_-, V_H = W_H, Z_H, A_H). \quad (3.5)$$

The explicit expressions for the LO partial decay widths of  $T$ -odd up- and down-type mirror quarks,  $\Gamma_{LO}(q_- \rightarrow V_H q')$ , can be found in Appendix B of Ref.[16].

### III.4 Checks

The verification of the correctness of our calculations are made in the following ways: Firstly, we employ the same PDFs and input parameters as used in Ref.[14] to calculate the LO cross section. The numerical results we obtained are in good agreement with those shown in Fig.6 of Ref.[14]. Secondly, we check the cancelations of UV and IR divergences both analytically and numerically. Finally, we check the independence of the NLO QCD corrected total cross section on the soft cutoff  $\delta_s$  in the range of  $5 \times 10^{-6} < \delta_s < 5 \times 10^{-3}$  with  $\delta_c = \delta_s/100$ . That is a good indirect check for the correctness of our evaluations. In the further numerical calculations, we set  $\delta_s = 5 \times 10^{-5}$  and  $\delta_c = 5 \times 10^{-7}$ .



## IV. Numerical results and discussions

### IV..1 Input parameters

In this section we present and discuss the numerical results for the same-sign  $T$ -odd mirror quark pair production of the first two generations at both the LO and the QCD NLO. The SM input parameters for our calculations are taken as [31]

$$\alpha_{ew}^{-1} = 137.036, \quad m_W = 80.385 \text{ GeV}, \quad m_Z = 91.1876 \text{ GeV}. \quad (4.1)$$

The Weinberg angle is fixed in the on-shell scheme as  $\sin^2 \theta_W = 1 - (\frac{m_W}{m_Z})^2 = 0.2229$ . We adopt the CTEQ6L1 PDFs and CTEQ6.6 PDFs [30] for the LO and QCD NLO calculations, separately. We take one-loop and two-loop running  $\alpha_s$  in the LO and QCD NLO calculations [31], and the strong coupling constant  $\alpha_s(\mu)$  is determined by the QCD parameter  $\Lambda_5^{LO} = 165 \text{ MeV}$  for the CTEQ6L1 at the LO and  $\Lambda_5^{\overline{MS}} = 226 \text{ MeV}$  for the CTEQ6.6 at the QCD NLO [31], respectively. The factorization and the renormalization scales are set to be equal ( $\mu_f = \mu_r = \mu$ ) for simplicity, and the central scale value is defined as  $\mu_0 = (m_{u-} + m_{d-})$ . The masses for the light quarks ( $u, d, c, s$ ) are set to be zero in our numerical calculations.

### IV..2 Integrated cross sections

In Fig.2 we show the dependence of the LO, NLO QCD corrected total cross sections and the QCD  $K$ -factor on the factorization/renormalization scale for the same-sign  $T$ -odd mirror quark pair production of all the first two generations at the LHC14. The LHT parameters are taken as  $f = 700 \text{ GeV}$  and  $\kappa = 1$ . From this figure we can see that at the central scale  $\mu_0$  the LO and NLO QCD corrected total cross sections are  $243.0 \text{ fb}$  and  $273.1 \text{ fb}$ , separately, and the corresponding  $K$ -factor ( $K \equiv \frac{\sigma_{NLO}}{\sigma_{LO}}$ ) is 1.12. If we define the upper and lower relative scale uncertainties as

$$\eta_{\text{upper}} = \frac{\max[\sigma(\mu) - \sigma(\mu_0)]}{\sigma(\mu_0)}, \quad \eta_{\text{lower}} = \frac{\min[\sigma(\mu) - \sigma(\mu_0)]}{\sigma(\mu_0)}, \quad \mu \in [\mu_0/4, 4\mu_0], \quad (4.2)$$

the relative scale uncertainties of the LO and NLO total cross sections are  $\left(\begin{smallmatrix} +19.0\% \\ -14.3\% \end{smallmatrix}\right)$  and  $\left(\begin{smallmatrix} +2.0\% \\ -4.5\% \end{smallmatrix}\right)$ , respectively. We see from Fig.2 and above data that the NLO QCD correction reduces the scale uncertainty significantly.

PDF is another source of theoretical uncertainty. In this work we consider the PDF uncertainty at the QCD NLO at the central scale  $\mu_0$ . For a given parametrization of the PDFs, the PDF uncertainty

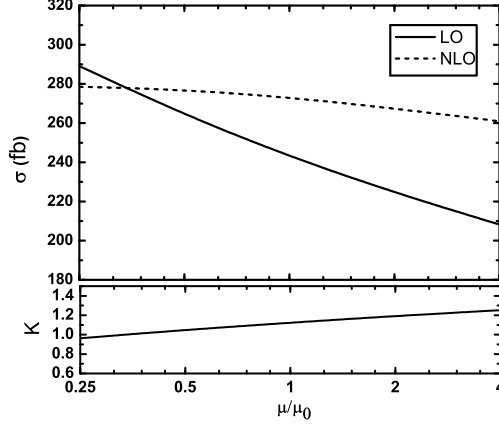


Figure 2: The dependence of the LO, NLO QCD corrected total cross sections and the QCD  $K$ -factor on the factorization/renormalization scale for the  $pp \rightarrow q_- q'_- + X$  process at the LHC14.

comes from the experimental uncertainties on the fitted data. We employ the definition of PDF uncertainty on the hadronic cross section given in Ref.[32]. By making use of the 44 additional PDF sets provided by the CTEQ6.6, we obtain the NLO QCD corrected integrated cross section with the PDF uncertainty at  $\mu = \mu_0$  as  $\sigma_{NLO} = 273.1^{+9.8}_{-8.3} fb$ . The corresponding relative PDF uncertainties are  $\left( \begin{smallmatrix} +3.6\% \\ -3.0\% \end{smallmatrix} \right)$ , which are of the same level as the relative scale uncertainties at the QCD NLO. By adding linearly the scale and PDF uncertainties, the NLO integrated cross section at  $\mu = \mu_0$  is  $\sigma_{NLO} = 273.1^{+5.4}_{-12.2} {}^{+9.8}_{-8.3} fb = 273.1^{+15.2}_{-20.5} fb$ . Although we consider both the scale uncertainty and PDF uncertainty for the NLO QCD corrected integrated cross section, the combined uncertainty is still much smaller than the LO scale uncertainty, which has the value of  $\sigma_{LO} = 243.0^{+46.1}_{-34.7} fb$  at  $\mu = \mu_0$ .

The dependence of the LO, NLO QCD corrected total cross sections and the QCD  $K$ -factor on the global symmetry breaking scale  $f$  are depicted in Fig.3, with  $\kappa = 1$  and  $f$  varying from 500 GeV to 2 TeV. The figure shows that the LO integrated cross section is 1213.2 fb at  $f = 500$  GeV, and decreases rapidly to 0.173 fb at  $f = 2$  TeV. The NLO QCD corrected integrated cross section has the same tendency as the LO cross section, having the values of  $\sigma_{NLO} = 1382.8 fb$  at  $f = 500$  GeV and  $\sigma_{NLO} = 0.186 fb$  at  $f = 2$  TeV. This sensitive dependence of both the LO and NLO QCD corrected integrated cross sections for the  $pp \rightarrow q_- q'_- + X$  process on the parameter  $f$  is clearly displayed in Fig.3. It can be explained by that with the increment of the global symmetry breaking scale  $f$ , the masses of  $T$ -odd mirror quarks become heavier, which suppresses the phase space of final state. The

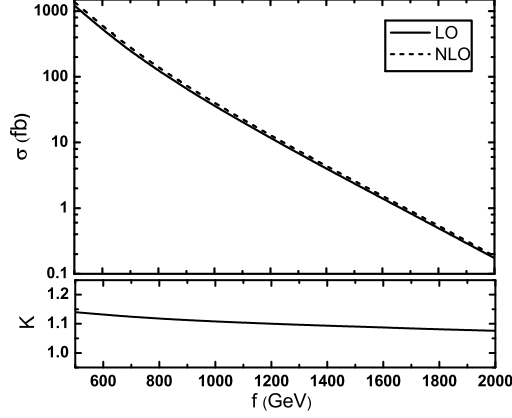


Figure 3: The dependence of the LO, NLO QCD corrected total cross sections and the QCD  $K$ -factor on the global symmetry breaking scale  $f$  for the  $pp \rightarrow q_- q'_- + X$  process at the LHC14.

QCD  $K$ -factor varies from 1.14 to 1.08 as the increment of  $f$  from 500 GeV to 2 TeV, and exhibits weak dependence on the global symmetry breaking scale  $f$ .

In Fig.4 we present the LO, NLO QCD corrected total cross sections and the QCD  $K$ -factor for the same-sign  $T$ -odd mirror quark pair production of all the first two generations at the LHC14 as functions of the  $T$ -odd mirror quark Yukawa coupling  $\kappa$  by taking  $f = 700$  GeV. A similar behavior as depicted in Fig.3 can be found in Fig.4. It is because the  $T$ -odd mirror quark mass is simultaneously proportional to the parameters  $\kappa$  and  $f$  as shown in Eq.(2.5). The LO integrated cross sections are 1064.4 fb and 102.8 fb, while the NLO QCD corrected integrated cross sections are 1357.1 fb and 111.7 fb, at  $\kappa = 0.5$  and  $\kappa = 1.5$ , respectively. The corresponding  $K$ -factor decreases from 1.27 to 1.09 when  $\kappa$  varies from 0.5 to 1.5, which shows that the  $K$ -factor is more sensitive to the Yukawa coupling  $\kappa$  than to the global symmetry breaking scale  $f$ .

### IV..3 Distributions of final products

From Eqs.(2.3) and (2.5) we know that we have the mass spectrum with  $m_{q_-} > m_{W_H} > m_{A_H}$  and  $A_H$  being the lightest  $T$ -odd particle by setting  $\kappa > 0.45$  [13]. In the following we take  $\mu = \mu_0$ ,  $f = 700$  GeV and  $\kappa = 1$  only for demonstration. In this case we get  $m_{u_-} = m_{c_-} = 974.67$  GeV,  $m_{d_-} = m_{s_-} = 989.95$  GeV,  $m_{W_H} = m_{Z_H} = 442.06$  GeV and  $m_{A_H} = 99.24$  GeV. Then the main decay modes of the  $T$ -odd mirror quark  $q_-$  are  $q_- \rightarrow W_H q'$ ,  $q_- \rightarrow Z_H q$  and  $q_- \rightarrow A_H q$ . We assume that the total decay width of  $q_-$  is the summation of the partial decay widths of these three decay modes, i.e.,

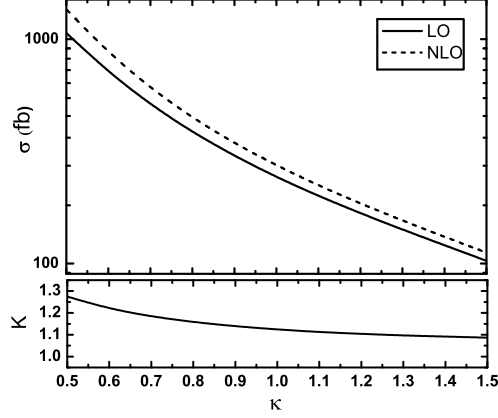


Figure 4: The dependence of the LO, NLO QCD corrected total cross sections and the QCD  $K$ -factor on the  $T$ -odd mirror quark Yukawa coupling  $\kappa$  for the  $pp \rightarrow q_- q'_- + X$  process at the LHC14.

$\Gamma_{q_-}^{\text{tot}} = \Gamma(q_- \rightarrow W_H q') + \Gamma(q_- \rightarrow Z_H q) + \Gamma(q_- \rightarrow A_H q)$ . By adopting the decay width expressions in Eq.(3.5), we obtain the branch ratios for these decay channels as

$$\begin{aligned} Br(U_- \rightarrow W_H D, Z_H U, A_H U) &= 59.84\%, 29.80\%, 10.36\%, \\ Br(D_- \rightarrow W_H U, Z_H D, A_H D) &= 62.87\%, 31.55\%, 5.58\%, \end{aligned} \quad (4.3)$$

where  $U$  and  $D$  are the up- and down-type SM quarks of the first two generations, and  $U_-$  and  $D_-$  are the corresponding  $T$ -odd mirror quarks. Via the following cascade decays of the  $T$ -odd mirror quarks,

$$\begin{aligned} U_- &\rightarrow W_H D \rightarrow W A_H D \rightarrow \ell \nu A_H D, \\ D_- &\rightarrow W_H U \rightarrow W A_H U \rightarrow \ell \nu A_H U, \quad (\ell = e^\pm, \mu^\pm, \quad \nu = \nu_e, \bar{\nu}_e, \nu_\mu, \bar{\nu}_\mu), \end{aligned} \quad (4.4)$$

the same-sign  $T$ -odd mirror quark pair production gives rise to the interesting same-sign dilepton signature associated with jets and a significant amount of missing energy,

$$pp \rightarrow q_- q'_- \rightarrow \ell^\pm \ell'^\pm + jets + \cancel{E}_T + X, \quad (\ell^\pm \ell'^\pm = e^\pm e^\pm, \mu^\pm \mu^\pm, e^\pm \mu^\pm). \quad (4.5)$$

In our numerical calculations we take  $Br(W \rightarrow e \nu_e) = 10.75\%$  and  $Br(W \rightarrow \mu \nu_\mu) = 10.57\%$  [31]. All the kinematic distributions for the same-sign dilepton signal process (4.5) investigated in our paper are summed over  $e^\pm e^\pm$ ,  $\mu^\pm \mu^\pm$  and  $e^\pm \mu^\pm$  final states.<sup>1</sup>

<sup>1</sup> Besides the kinematic distributions for the signal process in Figs.5-8, the  $H_T$  distribution for the SM background process  $pp \rightarrow W^\pm W^\pm q q' \rightarrow \ell^\pm \ell'^\pm + 2 jets + \cancel{E}_T + X$  in Fig.8(a) is also summed over  $e^\pm e^\pm$ ,  $\mu^\pm \mu^\pm$  and  $e^\pm \mu^\pm$  final states.

Among the two same-sign leptons in final state, the leading lepton  $\ell_1$  and the second lepton  $\ell_2$  are defined as

$$p_T^{\ell_1} > p_T^{\ell_2}. \quad (4.6)$$

For the jets originating from the decays of the produced same-sign  $T$ -odd mirror quarks and the real gluon/light-quark emissions, we merge the proto-jets to define the final jets by adopting the Cambridge/Aachen (C/A) jet algorithm [33], setting  $R = 0.7$ . After performing the jet merging procedure, there are three kinds of same-sign dilepton events at the QCD NLO, i.e.,  $\ell^\pm \ell'^\pm + 1 \text{ jet} + \cancel{E}_T$ ,  $\ell^\pm \ell'^\pm + 2 \text{ jets} + \cancel{E}_T$  and  $\ell^\pm \ell'^\pm + 3 \text{ jets} + \cancel{E}_T$ , for the same-sign  $T$ -odd mirror quark pair production. We define the jet with the largest transverse momentum in the two-jet or three-jet event as well as the only jet in the one-jet event as the leading jet, denoted as  $j_1$ . The final produced two heavy photons and two neutrinos can not be detected directly, and are manifested as the missing of transverse energy. We use the Monte Carlo method and adopt the narrow width approximation (NWA) to generate these signal events, as well as the background events used in the  $H_T$  distribution for the SM background (“background@LO” histogram in Fig.8(a)).

The LO, NLO QCD corrected transverse momentum distributions and corresponding  $K$ -factors of the leading lepton  $\ell_1$ , second lepton  $\ell_2$  and leading jet  $j_1$  are shown in Figs.5(a), (b) and (c), respectively. In the range of  $p_T^{\ell_1} \in [50, 350]$  GeV, the NLO QCD correction enhances the LO  $p_T^{\ell_1}$  distribution by more than 10%, and the  $K$ -factor is about 1.11 – 1.16. Both the LO and NLO QCD corrected  $p_T^{\ell_1}$  distributions reach their maxima at the position of  $p_T^{\ell_1} \sim 100$  GeV with  $K \sim 1.14$ . The  $p_T$  distributions of the second lepton are quite different from the corresponding distributions of the leading lepton. Both the LO and NLO QCD corrected  $p_T^{\ell_2}$  distributions peak at the position of  $p_T^{\ell_2} \sim 25$  GeV, while the  $K$ -factor of the  $p_T^{\ell_2}$  distribution seems to be similar with that of the  $p_T^{\ell_1}$  distribution. The NLO QCD correction also enhances the LO transverse momentum distribution of the leading jet for  $p_T^{j_1} > 100$  GeV, and the  $K$ -factor is about 1.09 – 1.18 in the range of  $p_T^{j_1} \in [250, 600]$  GeV. The peaks of the LO and NLO QCD corrected  $p_T^{j_1}$  distributions are located at  $p_T^{j_1} \sim 375$  GeV with  $K \sim 1.18$ . We also see from these figures that the NLO QCD correction is less than 18% for the  $p_T$  distributions of the leading lepton, second lepton and leading jet in the plotted  $p_T$  regions.

In Figs.6(a), (b) and (c) we depict the LO and NLO QCD corrected rapidity distributions of the

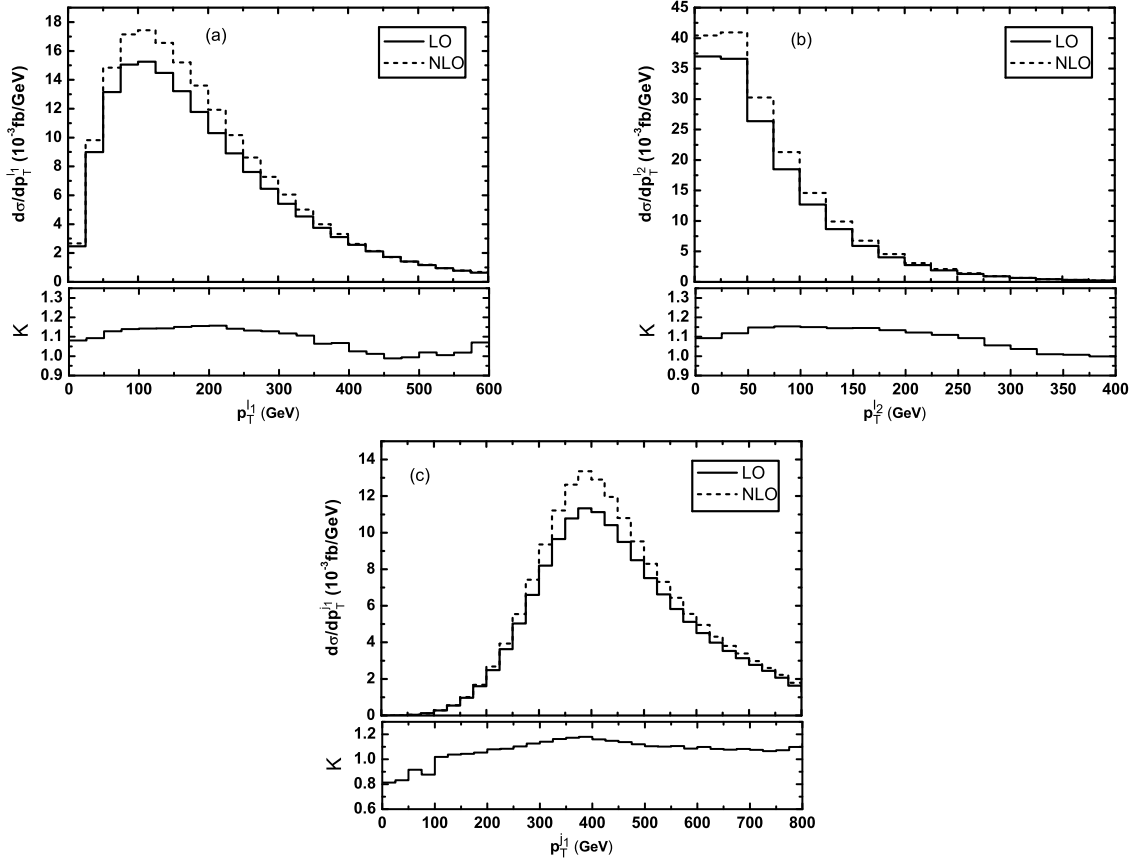


Figure 5: The LO, NLO QCD corrected transverse momentum distributions and corresponding  $K$ -factors for the  $pp \rightarrow q-q' \rightarrow \ell^\pm \ell'^\pm + jets + \cancel{E}_T + X$  process at the LHC14. (a) leading lepton  $\ell_1$ , (b) second lepton  $\ell_2$ , (c) leading jet  $j_1$ .

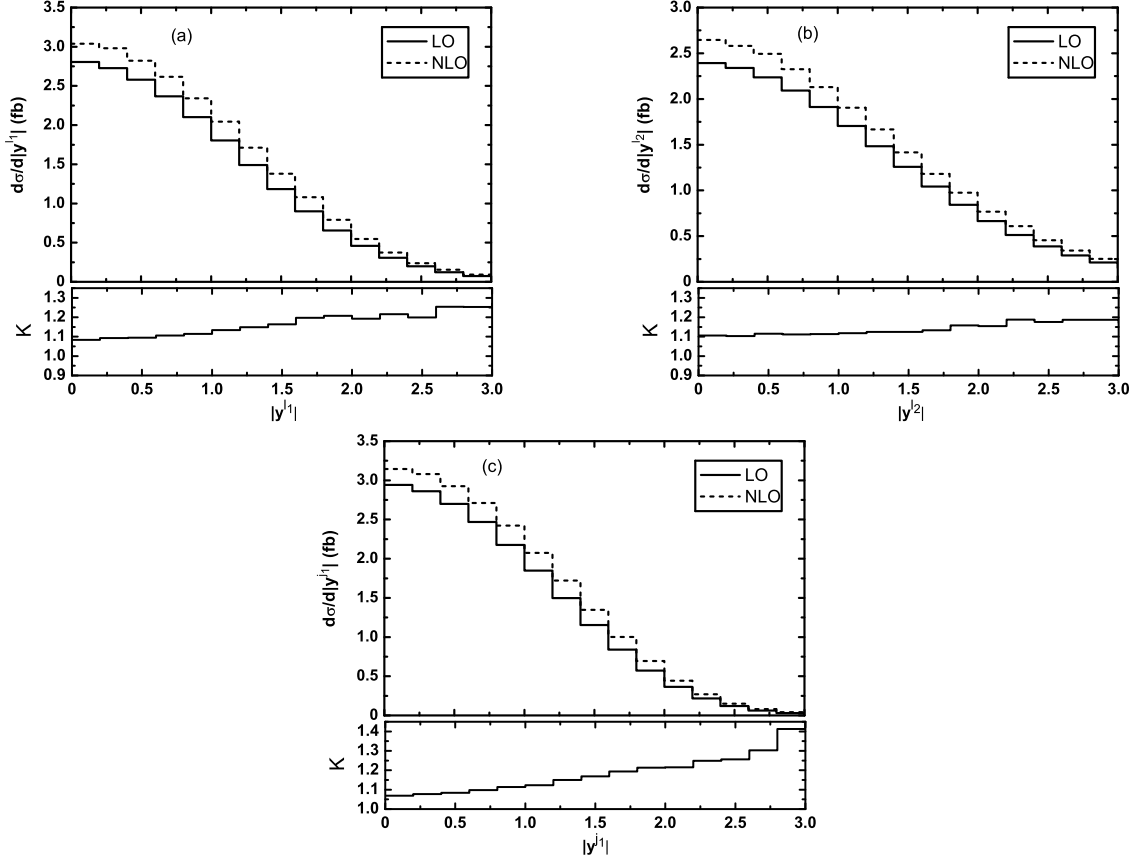


Figure 6: The LO, NLO QCD corrected rapidity distributions and corresponding  $K$ -factors for the  $pp \rightarrow q-q' \rightarrow \ell^\pm \ell'^\pm + jets + \cancel{E}_T + X$  process at the LHC14. (a) leading lepton  $\ell_1$ , (b) second lepton  $\ell_2$ , (c) leading jet  $j_1$ .

two same-sign leptons and leading jet, separately. We can see that all these rapidity distributions have similar behavior. The final two same-sign leptons and leading jet prefer to be produced in the central rapidity region. The  $K$ -factors in the three figures increase with the increment of  $|y|$ . For the leading jet rapidity distribution, the  $K$ -factor changes from 1.07 at  $|y^{j_1}| = 0$  to 1.41 at  $|y^{j_1}| = 3$ .

The LO and NLO QCD corrected distributions of the missing transverse momentum and invariant mass of two same-sign leptons in final state are presented in Figs.7(a) and (b), respectively. The missing transverse momentum is carried by the final two heavy photons and two neutrinos originating from the cascade decays of  $T$ -odd mirror quarks shown in Eq.(4.4). As shown in the two figures, both the LO and NLO QCD corrected missing transverse momentum distributions reach their maxima at  $p_T^{\text{miss}} \sim 275$  GeV with  $K \sim 1.13$ , and the LO and NLO QCD corrected invariant mass distributions of the same-sign lepton pair peak at  $M_{\ell\ell} \sim 50$  GeV with  $K = 1.08$ .

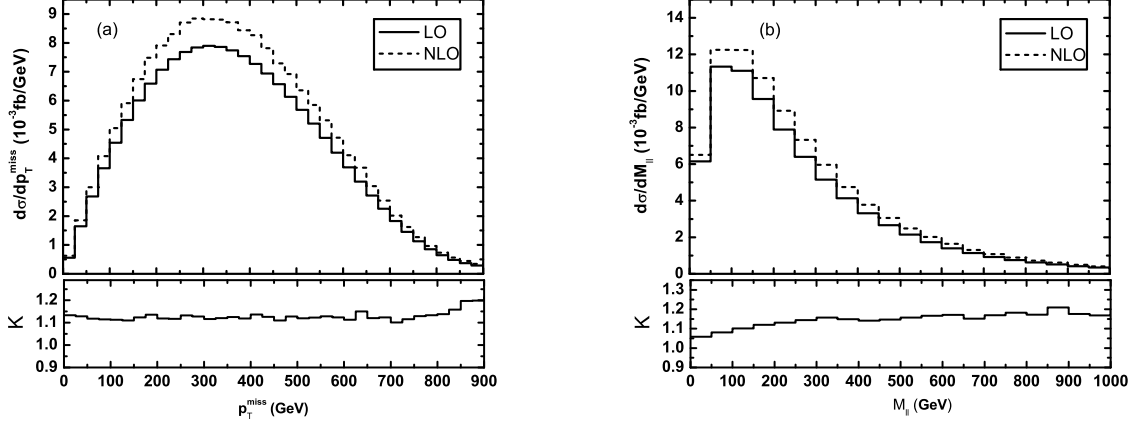


Figure 7: The LO and NLO QCD corrected distributions of the (a) missing transverse momentum  $p_T^{\text{miss}}$  and (b) invariant mass of same-sign lepton pair  $M_{\ell\ell}$ , for the  $pp \rightarrow q_- q'_- \rightarrow \ell^\pm \ell'^\pm + jets + \cancel{E}_T + X$  process at the LHC14.

In the following discussion we only consider the two-jet event,  $\ell^\pm \ell'^\pm + 2 jets + \cancel{E}_T$ , for the same-sign  $T$ -odd mirror quark pair production of the first two generations at the LHC. Then the SM background mainly comes from the same-sign  $W$  pair production in association with two light-quark jets, i.e.,  $pp \rightarrow W^\pm W^\pm qq' + X$ , followed by the subsequent leptonic  $W$  decays. We apply the exclusive event selection criteria, defined as

$$p_T^{j1} > 30 \text{ GeV}, \quad p_T^{j2} > 30 \text{ GeV}, \quad (4.7)$$

to select the events with two hard jets. In order to investigate the possibility of discriminating the signal of the same-sign  $T$ -odd mirror quark pair production from its SM background, we define  $H_T$  as the scalar sum of the transverse momenta of the two same-sign leptons, two hard jets and  $\cancel{E}_T$ ,

$$H_T = |\vec{p}_T^{\ell_1}| + |\vec{p}_T^{\ell_2}| + |\vec{p}_T^{j1}| + |\vec{p}_T^{j2}| + |\vec{p}_T^{\text{miss}}|, \quad (4.8)$$

for a given  $\ell^\pm \ell'^\pm + 2 jets + \cancel{E}_T$  event, and follow the way used in searching for the top quark at the Tevatron [34]. This kinematic variable is expected to be helpful for selecting the signal from the SM background.

The normalized  $H_T$  distributions for both the signal process  $pp \rightarrow q_- q'_- \rightarrow \ell^\pm \ell'^\pm + 2 jets + \cancel{E}_T + X$  at the QCD NLO and the SM background process  $pp \rightarrow W^\pm W^\pm qq' \rightarrow \ell^\pm \ell'^\pm + 2 jets + \cancel{E}_T + X$  at the LO are displayed in Fig.8(a). We can see from the figure that  $H_T$  distributions for the signal



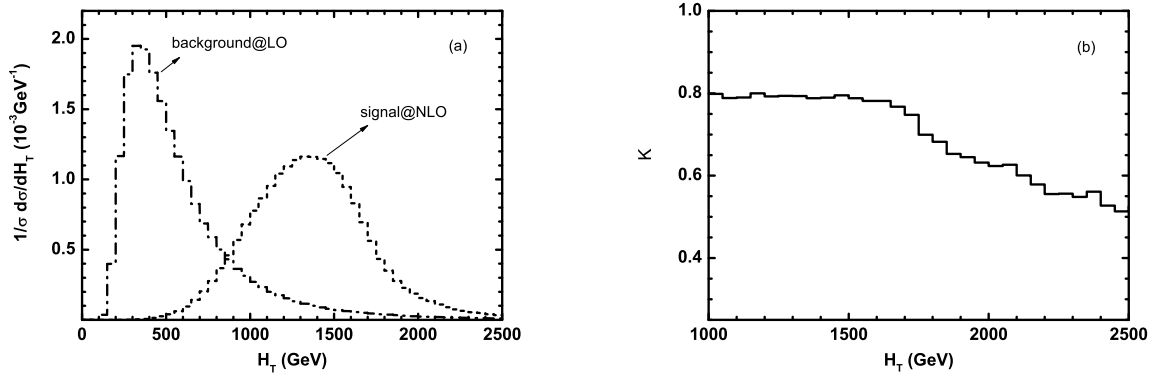


Figure 8: (a) The normalized  $H_T$  distributions for the signal process  $pp \rightarrow q-q' \rightarrow \ell^\pm \ell'^\pm + 2 \text{ jets} + \cancel{E}_T + X$  at the QCD NLO and the SM background process  $pp \rightarrow W^\pm W^\pm qq' \rightarrow \ell^\pm \ell'^\pm + 2 \text{ jets} + \cancel{E}_T + X$  at the LO at the LHC14. (b) The QCD  $K$ -factor of the  $H_T$  distribution for the signal process.

and SM background peak at  $H_T \sim 1.35$  TeV and  $H_T \sim 300$  GeV, respectively, and it is possible to distinguish between the desired signal of the same-sign  $T$ -odd mirror quark pair production and the SM background by adopting proper cut on  $H_T$ . In Fig.8(b) we plot the  $K$ -factor of the  $H_T$  distribution for the signal process. It shows that the NLO QCD correction to the  $H_T$  distribution is significant, particularly in the range of  $H_T > 1.7$  TeV. The  $K$ -factor varies from 0.80 to 0.51 with the increment of  $H_T$  from 1 TeV to 2.5 TeV. By comparing Figs.5-7 and Fig.8 we can see that the QCD correction depends strongly on the event selection scheme. Our numerical results show that the NLO QCD correction is positive in the inclusive scheme due to large positive contributions from the real gluon/light-quark emission processes, while it suppresses the LO  $H_T$  distribution in the exclusive scheme.

## V. Summary

In this paper we calculate the same-sign  $T$ -odd mirror quark pair production in the LHT at the  $\sqrt{s} = 14$  TeV LHC up to the QCD NLO. The theoretical uncertainties from the factorization/renormalization scale and PDFs are investigated. We find that the NLO QCD corrections reduce the scale uncertainty of the integrated cross section for the  $T$ -odd mirror quark pair production of the first two generations significantly. The upper and lower relative scale uncertainties of the total cross section at the central scale are  $\left( \begin{smallmatrix} +19.0\% \\ -14.3\% \end{smallmatrix} \right)$  at the LO, and are reduced to  $\left( \begin{smallmatrix} +2.0\% \\ -4.5\% \end{smallmatrix} \right)$  at the QCD NLO. We present the dependence

of the integrated cross section on the global symmetry breaking scale  $f$  and the  $T$ -odd mirror quark Yukawa coupling  $\kappa$ . We also provide the LO and NLO QCD corrected transverse momentum and rapidity distributions of the final products, including the leading lepton, second lepton, leading jet and missing energy, and the invariant mass distributions of the final produced same-sign lepton pair. Comparing the  $H_T$  distributions for the  $pp \rightarrow q_- q'_- \rightarrow \ell^\pm \ell'^\pm + 2 \text{ jets} + \cancel{E}_T + X$  and  $pp \rightarrow W^\pm W^\pm q q' \rightarrow \ell^\pm \ell'^\pm + 2 \text{ jets} + \cancel{E}_T + X$  processes, we find that the signal of the same-sign  $T$ -odd mirror quark pair production can be discriminated from the SM background via  $\ell^\pm \ell'^\pm + 2 \text{ jets} + \cancel{E}_T$  final state by adopting proper cut on the  $H_T$  parameter.

**Acknowledgments:** This work was supported by the National Natural Science Foundation of China (Grants. No.11275190, No.11375008, No.11375171).

## References

- [1] S. L. Glashow, Nucl. Phys. **22**, 579 (1961); S. Weinberg, Phys. Rev. Lett. **19**, 1264 (1967); A. Salam, Proc. 8th Nobel Symposium Stockholm 1968, ed. N. Svartholm (Almqvist and Wiksells, Stockholm 1968) p.367; H. D. Politzer, Phys. Rept. **14**, 129 (1974).
- [2] P. W. Higgs, Phys. Lett. **12**, 132 (1964), Phys. Rev. Lett. **13**, 508 (1964), Phys. Rev. **145**, 1156 (1966); F. Englert and R. Brout, Phys. Rev. Lett. **13**, 321 (1964); G. S. Guralnik, C. R. Hagen and T. W. B. Kibble, Phys. Rev. Lett. **13**, 585 (1964); T. W. B. Kibble, Phys. Rev. **155**, 1554 (1967).
- [3] R. Barbieri and A. Strumia, Phys. Lett. **B462**, 144 (1999).
- [4] G. Aad *et al.* (ATLAS Collaboration), Phys. Lett. **B716**, 1 (2012).
- [5] S. Chatrchyan *et al.* (CMS Collaborations), Phys. Lett. **B716**, 30 (2012).
- [6] N. Arkani-Hamed, A. G. Cohen, and H. Georgi, Phys. Lett. **B513**, 232 (2001); M. Schmaltz and D. Tucker-Smith, Annu. Rev. Nucl. Part. Sci. **55**, 229 (2005); M. Perelstein, Prog. Part. Nucl. Phys. **58**, 247 (2007), and references therein.
- [7] N. Arkani-Hamed, A. G. Cohen, E. Katz, and A. E. Nelson, JHEP **07** (2002) 034.

- [8] C. Csaki, J. Hubisz, G. D. Kribs, P. Meade and J. Terning, Phys. Rev. **D67**, 115002 (2003), Phys. Rev. **D68**, 035009 (2003); J. L. Hewett, F. J. Petriello and T. G. Rizzo, JHEP **10** (2003) 062; M. C. Chen and S. Dawson, Phys. Rev. **D70**, 015003 (2004); W. Kilian and J. Reuter, Phys. Rev. **D70**, 015004 (2004); Z. Han and W. Skiba, Phys. Rev. **D71**, 075009 (2005).
- [9] H. -C. Cheng and I. Low, JHEP **09** (2003) 051.
- [10] H. -C. Cheng and I. Low, JHEP **08** (2004) 061.
- [11] I. Low, JHEP **10** (2004) 067.
- [12] J. Hubisz and P. Meade, Phys. Rev. **D71**, 035016 (2005); J. Hubisz, P. Meade, A. Noble and M. Perelstein, JHEP **01** (2006) 135.
- [13] J. Reuter, M. Tonini and Maikel de Vries, JHEP **02** (2014) 053.
- [14] A. Belyaev, C. -R. Chen, K. Tobe and C. -P. Yuan, Phys. Rev. **D74**, 115020 (2006).
- [15] D. Choudhury, D. K. Ghosh and S. K. Rai, JHEP **07** (2012) 013; D. Choudhury and D. K. Ghosh, JHEP **08** (2007) 084; S. Mukhopadhyay, B. Mukhopadhyaya and A. Nyffeler, JHEP **05** (2010) 001.
- [16] S. -M. Du, L. Guo, W. Liu, W. -G. Ma and R. -Y. Zhang, Phys. Rev. **D86**, 054027 (2012).
- [17] W. Liu, R. -Y. Zhang, L. Guo, W. -G. Ma and L. -W. Chen, Phys. Rev. **D87**, 034034 (2013).
- [18] R. -Y. Zhang, H. Yan, W. -G. Ma, S. -M. Wang, L. Guo and L. Han, Phys. Rev. **D85**, 015017 (2012); X. -D. Yang, S. -J. Xiong, W. -G. Ma, R. -Y. Zhang, L. Guo and X. -Z. Li Phys. Rev. **D89**, 014008 (2014).
- [19] CMS Collaboration, JHEP **06** (2011) 077, JHEP **01** (2014) 163, Phys. Rev. Lett. **109**, 071803 (2012).
- [20] ATLAS Collaboration, Phys. Rev. Lett. **108**, 241802 (2012).
- [21] M. Blanke, A. J. Buras, A. Poschenrieder, S. Rehsiegel, C. Tarantino, S. Uhlig and A. Weiler, JHEP **01** (2007) 066.

- [22] T. Hahn, Comput. Phys. Commun. **140**, 418 (2001).
- [23] T. Hahn, M. Perez-Victoria, Comput. Phys. Commun. **118**, 153 (1999).
- [24] R. K. Ellis and G. Zanderighi, JHEP **02** (2008) 002.
- [25] G. t'Hooft and M. Veltman, Nucl. Phys. **B153**, 365 (1979).
- [26] A. Denner, U. Nierste and R. Scharf, Nucl. Phys. **B367**, 637 (1991).
- [27] A. Denner and S. Dittmaier, Nucl. Phys. **B658**, 175 (2003).
- [28] B. W. Harris and J. F. Owens, Phys. Rev. **D65**, 094032 (2002).
- [29] T. Kinoshita, J. Math. Phys. **3**, 650 (1962); T. D. Lee and M. Nauenberg, Phys. Rev. **133**, B1549 (1964).
- [30] J. Pumplin, D. R. Stump, J. Huston, H. -L. Lai, P. Nadolsky and W. -K. Tung, JHEP **07** (2002) 012; P. M. Nadolsky, H.-L. Lai, Q. -H. Cao, J. Huston, J. Pumplin, D. Stump, W. -K. Tung and C. -P. Yuan, Phys. Rev. **D78**, 013004 (2008).
- [31] J. Beringer *et al.* (Particle Data Group), Phys. Rev. **D86**, 010001 (2012).
- [32] G. Watt, JHEP **09** (2011) 069.
- [33] G. P. Salam, Eur. Phys. J. **C67**, 637 (2010).
- [34] S. Abachi *et al.* (D0 Collaboration), Phys. Rev. Lett. **74**, 2632 (1995); F. Abe *et al.* (CDF Collaboration), Phys. Rev. Lett. **74**, 2626 (1995).